ISSN 1674-1056
http://cpb.iphy.ac.cn
http://iopscience.iop.org/cpb
中国物理 B
Chinese Physics
中国物理
Chinese Physics B

Analysis of extreme ultraviolet spectral profiles of laser-produced Cr plasmas

L Wu(吴磊), M G Su(苏茂根), Q Min(敏琦), S Q Cao(曹世权), S Q He(何思奇), D X Sun(孙对兄), C Z Dong(董晨钟)

Citation: Chin. Phys. B . 2019, 28(7): 075201. **doi:** 10.1088/1674-1056/28/7/075201
Journal homepage: http://cpb.iphy.ac.cn; http://iopscience.iop.org/cpb

What follows is a list of articles you may be interested in

Factors affecting improvement of fluorescence intensity of quartet and doublet state of NO diatomic molecule excited by glow discharge

Ahmed Asaad I Khalil, Reem Al-Tuwirqi, Mohammed A Gondal, Noura Al-Suliman
Chin. Phys. B . 2018, 27(8): 085202. **doi:** 10.1088/1674-1056/27/8/085202

Laser-induced convenient fabrication of CdS nanocages with super-adsorption capability for methyl blue solution

Le Liu(刘乐), Lin-Lin Xu(徐林林), Hua Zhang(张华), Ming Chen(陈明)
Chin. Phys. B . 2017, 26(8): 085206. **doi:** 10.1088/1674-1056/26/8/085206

Femtosecond laser induced nanostructuring of zirconium in liquid confined environment

Nisar Ali, Shazia Bashir, Umm-i-Kalsoom, M. Shahid Rafique, Narjis Begum, Wolfgang Husinsky, Ali Ajami, Chandra S. R. Natahala
Chin. Phys. B . 2017, 26(1): 015204. **doi:** 10.1088/1674-1056/26/1/015204

Spectral and ion emission features of laser-produced Sn and SnO_2 plasmas

Hui Lan(兰慧), Xin-Bing Wang(王新兵), Du-Luo Zuo(左都罗)
Chin. Phys. B . 2016, 25(3): 035202. **doi:** 10.1088/1674-1056/25/3/035202

Mitigation of energetic ion debris from Gd plasma using dual laser pulses and the combined effect with ambient gas

Dou Yin-Ping, Sun Chang-Kai, Liu Chao-Zhi, Gao Jian, Hao Zuo-Qiang, Lin Jing-Quan
Chin. Phys. B . 2014, 23(7): 075202. **doi:** 10.1088/1674-1056/23/7/075202

Analysis of extreme ultraviolet spectral profiles of laser-produced Cr plasmas*

L Wu(吴磊), M G Su(苏茂根)†, Q Min(敏琦), S Q Cao(曹世权), S Q He(何思奇), D X Sun(孙对兄), and C Z Dong(董晨钟)‡

Key Laboratory of Atomic and Molecular Physics & Functional Material of Gansu Province, College of Physics and Electronic Engineering, Northwest Normal University, Lanzhou 730070, *China*

(Received 13 March 2019; revised manuscript received 27 April 2019; published online 31 May 2019)

Radiation from laser-produced plasmas was examined as a potential wavelength calibration source for spectrographs in the extreme ultraviolet (EUV) region. Specifically, the EUV emission of chromium (Cr) plasmas was acquired via spatio-temporally resolved emission spectroscopy. With the aid of Cowan and flexible atomic code (FAC) structure calculations, and a comparative analysis with the simulated spectra, emission peaks in the 6.5–15.0 nm range were identified as 3p–4d, 5d and 3p–4s transition lines from Cr^{5+}–Cr^{10+} ions. A normalized Boltzmann distribution among the excited states and a steady-state collisional-radiative model were assumed for the spectral simulations, and used to estimate the electron temperature and density in the plasma. The results indicate that several relatively isolated emission lines of highly charged ions would be useful for EUV wavelength calibration.

Keywords: laser-produced plasmas, highly charged ions, extreme ultraviolet, wavelength calibration

PACS: 52.38.Mf, 32.30.Jc, 52.70.Kz **DOI:** 10.1088/1674-1056/28/7/075201

1. Introduction

Laser-produced tin plasmas and gas-discharge xenon plasmas have been widely investigated because their compactness and high emissivity around 13.5 nm make them an attractive extreme ultraviolet light (EUV) source.[1–5] In previous studies, tin spectra in the 13.5 nm region show a complicated spectral profile with a broad reabsorption band and several pronounced dips. The true spectral profiles of tin ions in optically thick plasmas are distorted to yield the observed profile by self-absorption features owing to the opacity effect.[6] Meanwhile, the fact that more than tens of thousands of individual lines contribute to the quasi-continuum band or unresolved transition array (UTA) spectral profile in the EUV region presents a challenge to the accurate analysis of the EUV experimental spectra.[7] Therefore, a high-resolution EUV spectrograph is an indispensable tool to accurately determine the radiation properties and to analyze the evolution of the short-wavelength plasma light sources. However, most spectrographs require accurate wavelength calibrations before each measurement.[8–11]

The wavelength calibration of a spectrograph directly affects the spectral analysis. For example, grazing-incidence spectrographs disperse light with a grating while recording the spectrum with a charge-coupled device (CCD), and calibration is needed to determine the wavelength of each characteristic peak on the CCD. Each pixel of the detector corresponds to a specific wavelength, and calibration establishes the pixel–wavelength relationship. For wavelengths below 200 nm, the common calibration sources are hollow-cathode gas discharges,[12] multiple-anode sources,[13] and laser-produced plasmas (LPPs). Relative to LPPs, the other two sources are expensive and their calibration process is tedious.

LPPs have high densities and temperatures and consist of highly-charged ions. They emit intense radiation from the visible to x-rays,[14–20] and are typically produced by a high-energy pulsed (e.g., *Q*-switched) laser focused on a solid target. Highly charged ions of several low Z elements, such as C,[21] Si,[22,23] Al,[24,25] S,[26] and O,[27] have isolated spectral features in the EUV and soft-x-ray regions that offer good resolution and spectral characteristics typical of simple energy level structures. Therefore, they can be used as potential calibration sources for EUV spectrographs. However, due to the limited number of spectral lines from low Z elements in the EUV region, auxiliary calibration using isolated EUV spectra of middle Z elements is necessary.

In this paper, we demonstrate the wavelength calibration of a grazing incidence grating spectrograph with known spectral lines from C, Si, Al, and S LPPs. In addition, the EUV spectra of chromium (Cr) LPPs are analyzed to obtain spectral lines of highly charged ions for EUV wavelength calibration in the 6.5–15.0 nm range.

*Project supported by the National Key Research and Development Program of China (Grant No. 2017YFA0402300) and the National Natural Science Foundation of China (Grant Nos. 11874051, 11274254, and 11564037).

†Corresponding author. E-mail: nwnu_sumg@163.com

‡Corresponding author. E-mail: dongcz@nwnu.edu.cn

© 2019 Chinese Physical Society and IOP Publishing Ltd

2. Experimental setup and wavelength calibration of grazing incidence spectrograph in the EUV region

Details of the experimental setup for spatio-temporally resolved LPPs emission spectroscopy have been reported previously,[28] and will be briefly described here. A Nd : YAG laser (PRO-350, Spectra-Physics) with a fundamental wavelength of 1064 nm and pulse width of 10 ns was used to produce plasmas in a vacuum chamber by tightly focusing the beam on a planar Cr target. The EUV radiation was coupled into the 10 μm entrance slit of a 1.0 m focal length grazing incidence spectrograph (McPherson 310 G), equipped with a 600 grooves/mm grating. The dispersed spectra were detected with a 40 mm diameter micro channel plate (MCP) detector coupled via a coherent fiber-optic bundle to a 1024×255 pixel charge coupled device. The spectra were temporally resolved by gating the MCP with a negative voltage pulse (-2200 V) for a minimum width of 60 ns. The spectrograph covered the spectral region of 6.6–68 nm via a Rowland circle. Here, the spectral measured range was fixed over 6.5–15 nm, corresponding to resolving powers ($\lambda/\Delta\lambda$) from 361 to 4286, respectively.

To obtain the dispersion function of the spectrometer, well-known lines from highly charged C, Al, Si, and S, and their higher-order diffractions were used to cover the whole wavelength range of interest, as shown by the symbols in Fig. 1(a). Several peaks were deconvoluted before wavelength calibration so that the relationship between the transition wavelength and peak pixel could be accurately determined. These included two Si peaks at 11.79 nm and 11.90 nm, two Al peaks at 12.52 nm and 13.05 nm, and three S peaks at 7.24 nm, 14.53 nm, and 14.63 nm, which have been indicated in Fig. 1. A total of twelve lines were used in the calibration with wavelength values taken from the National Institute of Standards and Technology (NIST) atomic spectra database (ASD).[24] A parabolic polynomial was used to fit the pixel versus wavelength calibration, as plotted in Fig. 1(b). Multiple measurements and calibrations revealed that the calibration parameters were constant. This dispersion function was also used to calibrate the Cr spectra.

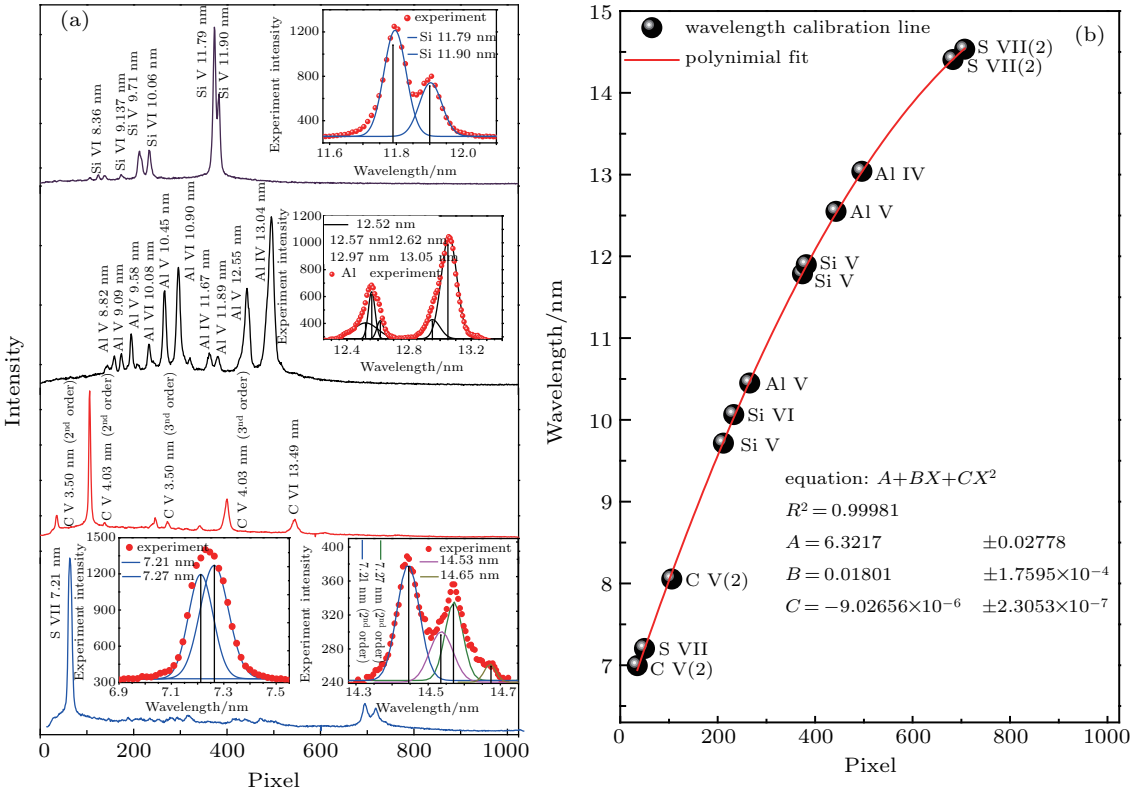


Fig. 1. Experimental spectra and wavelength calibration. (a) Spectral profile analysis based on known spectral lines of laser-produced C, Si, Al, and S plasmas, (b) polynomial fitting.

3. Analysis of EUV spectral profiles of laser-produced Cr plasmas

To avoid line shifts and to reduce opacity effects on the spectral profiles, the entrance slit width was set to 10 μm, and the MCP gate width was set to 60 ns. Figure 2(a) shows a spectrum in the 6.5–15.0 nm range produced with a laser intensity of 2.0×10^{11} W/cm^2. The spectrum was recorded at a location 1.5 mm away from the target surface and at a 55-ns time delay. To obtain accurate values of the central wavelengths and intensities, each peak was decomposed into Gaussian peaks by single- or multi-peak fitting methods. As dis-

played in Fig. 2(b), 36 preliminary lines were obtained according to the symmetry of the spectral peak profiles.

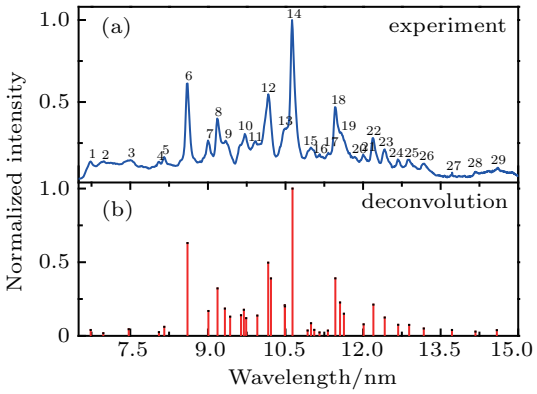


Fig. 2. Laser-produced Cr plasmas spectrum in the 6.5–15 nm wavelength range: (a) experimental spectrum and (b) decomposed lines.

From the perspective of atomic structure analysis, the experimental peaks in the spectra were identified via the NIST database and Hartree–Fock calculations of the Cowan RCN, RCN2, and RCG suites with configuration interaction codes and the flexible atomic code (FAC).[29–31] For the energy levels, wavelengths, weighted oscillator strengths, and transition probabilities, the excited-state basis contained $3s^2 3p^5 3d4s/4d$ (for Cr^{5+}), $3s^2 3p^k ns$, $3s^2 3p^k nd$ ($n = 4,5$, $k = 5$ for Cr^{6+}, $k = 4$ for Cr^{7+}, $k = 3$ for Cr^{8+}, $k = 2$ for Cr^{9+}, and $k = 1$ for Cr^{10+}). To optimize the output, the Slater–Condon integrals (F^k, G^k, and R^k) were reduced to 87%, while the spin parameter (ξ) was retained. In comparison, the emission lines could be identified from the 3p–4s, 4d, 5d transitions lines of Cr^{5+}–Cr^{10+} ions.

In the experimental and simulated comparative analysis, a steady-state collisional-radiative model was used to calculate the ion fractions at different ionization stages as a function of electron temperature and electron density.[32] Figures 3(a) and 3(b) plot the ion fractions of Cr^{5+}–Cr^{10+} ions as a function of electron temperature assuming an electron density $N_e = 6.4 \times 10^{20}$ cm^{-3}, and as a function of electron density assuming an electron temperature $T_e = 28.2$ eV, respectively. It is apparent that the electron temperature in the 15–43 eV range and the electron density in the 10^{19}–10^{21} cm^{-3} range can produce Cr^{5+}–Cr^{10+} ions.

In order to reproduce the experimental spectra and find the relationships between the experimental conditions and plasma parameters, a series of simulated spectra as a function of T_e and N_e have been obtained and compared with the experimental spectrum. Here, the total emission line profile was obtained by weighting and summing the corresponding Boltzmann factors and ion fractions for each ion and by convolving each line with a Gaussian function with a full width at half maximum (FWHM) of 0.09 nm. After comparison, a simulated spectrum closer to the experimental profile could be obtained. Usually, a minimum value among the deviations was less than 5%. This means that the best estimated value of the plasma temperature and electron density was obtained. Figure 4 shows the comparisons among the experimental spectrum and simulated spectra for an electron

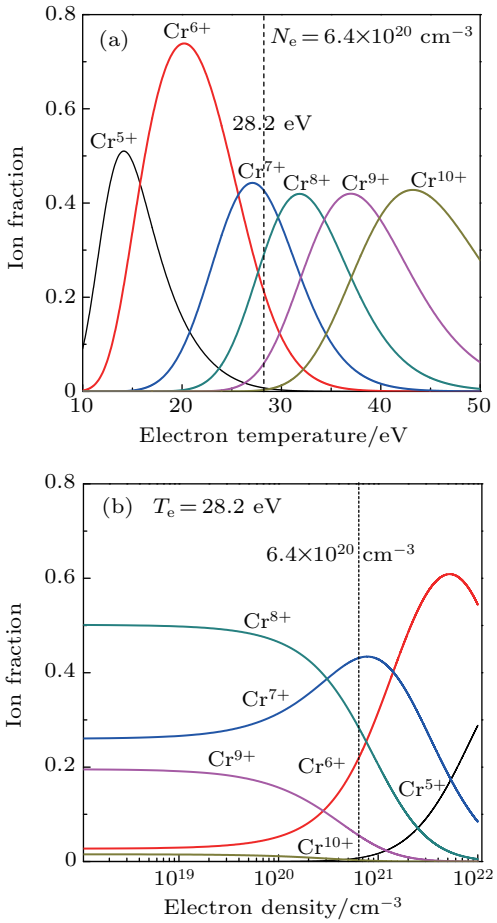


Fig. 3. Cr plasma charge-state ion fractions as a function of (a) electron temperature and (b) density. The vertical dashed lines show the relative ion fraction of different charge-state at an assumed electron temperature and electron density.

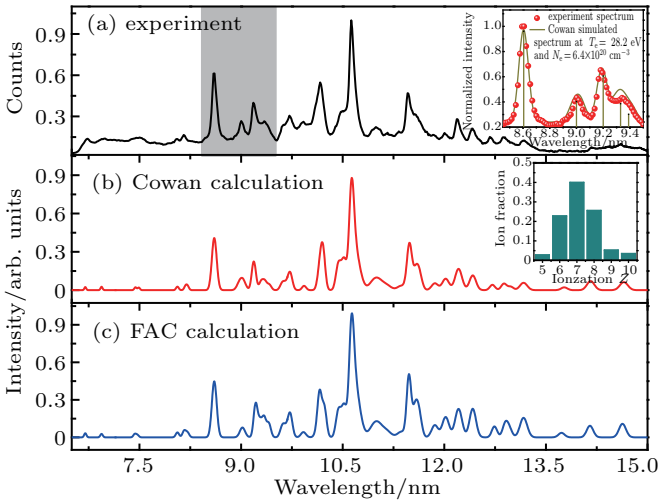


Fig. 4. Comparison between measured and simulated spectra: (a) experimental spectrum, (b) Cowan simulated spectrum, and (c) FAC simulated spectrum.

temperature of 28.2 eV and an electron density of 6.4×10^{20} cm^{-3}. Figure 4(a) shows the experimental spectrum recorded at a location 1.5 mm away from the target surface and at a 55 ns time delay. Figures 4(b) and 4(c) show the simulated spectra based on the atomic data from Cowan and FAC calculations, respectively. To realize mutual benchmark of Cowan and FAC calculations, the simulated spectra in Figs. 4(b) and 4(c) were obtained based on the same ion fractions and energy level populations. The inset bar chart shows the calculated ion fractions as a function of ionization stage. It can be seen by comparison that there is good agreement between the experimental and two simulated spectra, especially for wavelengths and intensities of intense lines from dominant ions. The respective fractional contributions of Cr^{5+}–Cr^{10+} ions were about 2.8%, 22.8%, 40%, 25.6%, 5.3%, and 3.5%.

Table 1 summarizes the observed and identified wavelengths, as well as other transition data that could be used for spectral simulations and comparative analysis. The data are arranged in order of wavelength, while the experimental wavelengths obtained by deconvolution are listed in the fourth column. The identified wavelengths obtained from the NIST database and calculated from FAC and Cowan codes are listed in the fifth to seventh columns. The final two columns give the transition probabilities from the FAC and Cowan calculations, which may be useful for future measurements of lifetimes and plasma spectra.

Table 1. Summary of measured and calculated data. The same number with different postscripts (in the first column) denotes the blending lines, the "*" indicates the new lines.

Index	Ion	Classification	Wavelength/nm				Transition probability	
			Exp.	NIST	Calc. (FAC)	Calc. (Cowan)	gA(FAC)/10^{10}	gA(Cowan)/10^{10}
1*	Cr^{10+}	$3s^23p^{23}P_1$-$3s^23p^15d^3P_2$	6.73±0.02		6.71	6.70	40.9	36.9
2*	Cr^{10+}	$3s^23p^{23}P_1$–$3s^23p^15d^3P_0$	6.94±0.02		6.94	6.94	38.9	40.4
3*	Cr^{10+}	$3s^23p^{21}D_2$–$3s^23p^15d^3F_2$	7.49±0.05		7.47	7.50	4.00	4.29
4	Cr^{10+}	$3s^23p^{23}P_0$–$3s^23p^14d^3D_1$	8.05±0.07	8.10	8.06	8.06	9.98	9.87
5	Cr^{10+}	$3s^23p^{21}D_2$–$3s^23p^14d^2F_3$	8.17±0.06	8.21	8.21	8.23	24.9	11.8
6*	Cr^{9+}	$3s^23p^{34}S_{3/2}$–$3s^23p^24d^2P_{1/2}$	8.62±0.04		8.62	8.61	5.89	6.20
7*	Cr^{9+}	$3s^23p^{32}P_{3/2}$–$3s^23p^24d^2D_{5/2}$	9.02±0.02		9.01	9.02	3.28	3.96
8*	Cr^{8+}	$3s^23p^{43}P_1$–$3s^23p^34d^3P_0$	9.18±0.03		9.19	9.20	2.56	2.13
9a*	Cr^{8+}	$3s^23p^{41}D_2$–$3s^23p^34d^1D_2$	9.33±0.07		9.31	9.35	2.36	2.20
9b	Cr^{8+}	$3s^23p^{43}P_1$–$3s^23p^34d^3D_2$	9.38±0.07	9.43	9.43	9.45	1.85	1.73
10a	Cr^{8+}	$3s^23p^{41}D_2$–$3s^23p^34d^1D_2$	9.62±0.05	9.65	9.64	9.64	1.26	1.19
10b	Cr^{8+}	$3s^23p^{43}P_2$–$3s^23p^34d^3D_3$	9.71±0.06	9.72	9.71	9.68	2.59	2.37
10c	Cr^{8+}	$3s^23p^{43}P_2$–$3s^23p^34d^3D_2$		9.80	9.74	9.77	2.54	2.67
11	Cr^{10+}	$3s^23p^{21}P_1$–$3s^23p^14s^3P_1$	9.93±0.05	9.95	9.92	9.93	22.8	21.7
12a	Cr^{7+}	$3s^23p^{52}P_{3/2}$–$3s^23p^44d^2D_{5/2}$	10.19±0.07	10.25	10.22	10.23	3.84	3.94
12b*	Cr^{7+}	$3s^23p^{52}P_{3/2}$–$3s^23p^44d^2P_{1/2}$			10.26	10.26	5.09	5.19
13	Cr^{7+}	$3s^23p^{52}P_{3/2}$–$3s^23p^44d^2D_{5/2}$	10.53±0.05	10.57	10.54	10.54	4.48	4.16
14	Cr^{7+}	$3s^23p^{52}P_{1/2}$–$3s^23p^44d^2D_{3/2}$	10.64±0.04	10.67	10.66	10.63	6.99	6.11
15a	Cr^{9+}	$3s^23p^{32}D_{5/2}$–$3s^23p^24s^2P_{3/2}$	10.95± 0.04	10.98	10.94	10.95	3.50	2.59
15b	Cr^{9+}	$3s^23p^{32}D_{3/2}$–$3s^23p^24s^2P_{1/2}$	11.01±0.06	11.04	11.03	11.02	5.21	4.84
15c	Cr^{9+}	$3s^23p^{32}P_{3/2}$–$3s^23p^24s^2D_{5/2}$		11.11	11.10	11.10	3.89	3.50
16*	Cr^{9+}	$3s^23p^{32}D_{3/2}$–$3s^23p^24s^4P_{1/2}$	11.20±0.05		11.22	11.19	3.29	2.18
17	Cr^{9+}	$3s^23p^{32}P_{1/2}$–$3s^23p^24s^2P_{1/2}$	11.39±0.03	11.37	11.40	11.37	3.34	2.33
18	Cr^{6+}	$3s^23p^{61}S_0$–$3s^23p^54d^1P_{1/2}$	11.51±0.05	11.54	11.50	11.51	4.99	4.46
19a	Cr^{6+}	$3s^23p^{63}P_1$–$3s^23p^54d^3D_0$	11.61±0.07	11.67	11.61	11.62	4.29	4.46
19b*	Cr^{6+}	$3s^23p^{61}S_0$–$3s^23p^54d^3P_1$			11.67	11.66	4.48	6.11
20	Cr^{8+}	$3s^23p^{43}P_1$–$3s^23p^34s^3D_2$	11.91±0.05	11.93	11.90	11.91	1.04	1.05
21	Cr^{8+}	$3s^23p^{41}D_2$–$3s^23p^34s^1D_2$	12.10±0.06	12.13	12.09	12.12	2.57	2.42
22	Cr^{8+}	$3s^23p^{41}S_0$–$3s^23p^34s^1P_1$	12.26±0.04	12.27	12.26	12.27	3.73	3.54
23	Cr^{7+}	$3s^23p^{52}P_{3/2}$–$3s^23p^44s^2S_{1/2}$	12.47±0.04	12.42	12.47	12.49	3.11	2.94
24*	Cr^{5+}	$3p^63d^2D_{5/2}$–$3p^53d4d^2D_{5/2}$	12.73±0.03		12.74	12.71	26.3	28.7
25*	Cr^{5+}	$3p^63d^2D_{5/2}$–$3p^53d4d^2P_{3/2}$	12.92±0.03		12.91	12.94	37.1	35.5
26	Cr^{7+}	$3s^23p^{52}P_{3/2}$–$3s^23p^44s^2P_{1/2}$	13.19±0.02	13.23	13.21	13.23	2.85	2.78
27*	Cr^{5+}	$3p^63d^{12}D_{3/2}$–$3p^53d4s^2P_{1/2}$	13.72±0.02		13.73	13.77	40.9	36.9
28*	Cr^{6+}	$3s^23p^{61}S_0$–$3s^23p^54d^3P_2$	14.15±0.02		14.15	14.13	3.01	2.85
29	Cr^{6+}	$3s^23p^{61}S_0$–$3s^23p^54d^1P_2$	14.59±0.06	14.65	14.63	14.65	2.83	2.64

Only transition probabilities from the FAC and Cowan calculated results are listed in Table 1 because of the absence of transition probabilities in the NIST ASD. A total of 29 peaks were classified, including 14 new lines. The peaks were attributed to 3p–4d, 5d, and 3p–4s transitions from Cr^{5+}–Cr^{10+} ions. The intense sharp peaks at 8.62 nm and 9.02 nm were attributed to the $3s^23p^{34}S_{3/2}$–$3s^23p^24d^2P_{1/2}$ and $3s^23p^{32}P_{3/2}$–$3s^23p^24d^2D_{5/2}$ transitions of Cr^{9+}, respectively,

the peaks at 9.18 nm and 12.26 nm were attributed to the $3s^2 3p^{43}P_1$–$3s^2 3p^3 4d^3P_0$ and $3s^2 3p^{41}S_0$–$3s^2 3p^3 4s^1P_1$ transitions of Cr^{8+}, respectively, the sharp peak at 10.64 nm was attributed to the $3s^2 3p^{52}P_{1/2}$–$3s^2 3p^4 4d^2D_{3/2}$ transition of Cr^{7+}, and the peak at 11.51 nm was attributed to the $3s^2 3p^{61}S_0$–$3s^2 3p^5 4d^1P_{1/2}$ transition of Cr^{6+}. Figure 5 shows a parabolic polynomial by fitting the pixel versus wavelength calibration using the lines of highly-charged Cr ions. This dispersion function was also used to calibrate the Cr spectra. With adequate resolution, these lines could be used for EUV spectrograph calibration.

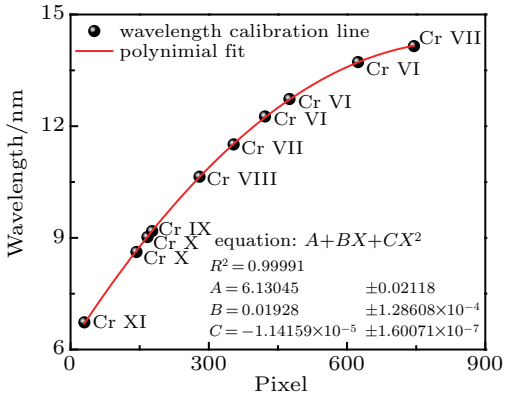


Fig. 5. Fitting the pixel vs. wavelength calibration using the lines of highly-charged Cr ions.

4. Conclusion

Laser-produced Cr plasma radiation in the EUV region was investigated as an EUV wavelength calibration source. EUV emission spectra of Cr^{5+}–Cr^{10+} ions over 6.5–15.0 nm were acquired via spatio-temporally resolved emission spectroscopy. Using the line information from the NIST ASD and from Cowan and FAC calculations, the peaks were identified as 3p–4d, 3p–5d, and 3p–4s transitions of Cr^{5+}–Cr^{10+}ions. By using a normalized Boltzmann distribution among the excited states and a steady-state collision radiation model, the electron temperature and electron density and the charge states in the plasma were investigated. The Cowan and FAC simulation results agreed very well with the experimental spectra. In conclusion, the results indicate that relatively isolated lines of highly charged Cr ions can be used for EUV wavelength calibration.

References

[1] Izawa Y, Nishihara K, Tanuma H, Sasaki A, Murakami M, Sunahara A, Nishimura H, Fujioka S, Aota T, Shimada Y, Yamaura M, Nakatsuka M, Fujita H, Tsubakimoto K, Yoshida H, Miyanaga N and Mima K 2008 *J. Phys.: Conf. Ser.* **112** 042047

[2] Harilal S S, Tillack M S, Tao Y, O'Shay B, Paguio R and Nikroo A 2006 *Opt. Lett.* **31** 1549

[3] Ueno Y, Soumagne G, Sumitani A, Endo A and Higashiguchi T 2007 *Appl. Phys. Lett.* **91** 231501

[4] Hara H, Arai G, Dinh T H, Jiang W H, Miura T, Endo A, Ejima T, Li B W, Dunne P, O'Sullivan G, Sunahara A and Higashiguchi T 2015 *J. Appl. Phys.* **118** 193301

[5] Churilov S S and Ryabtsev A N 2006 *Phys. Scr.* **73** 614

[6] Fujioka S 2005 *Phys. Rev. Lett.* **95** 235004

[7] Hayden P, Cummings A, Murphy N, O'Sullivan G, Sheridan P, White J and Dunne P 2006 *J. Appl. Phys.* **99** 093302

[8] Liu K and Yu F H 2013 *Opt. Eng.* **52** 013603

[9] Martinsen P, Jordan B, Mcglone A, Gaastra P and Laurie T 2008 *Appl. Spectrosc.* **62** 1008

[10] Sun Y C, Huang C, Xia G, Jin S Q and Lu H B 2017 *J. Opt. Soc. Am. A* **34** 498

[11] Liang G Y, Zhao G, Zhong J Y, Li Y F, Liu Y Q, Dong Q L, Yuan X H, Jin Z and Zhang J 2008 *Astron. Astrophys. J. Suppl. Ser.* **177** 326

[12] Tseng C H, Ford J F, Mann C K and Vickers T J 1993 *Appl. Spectrosc.* **47** 1808

[13] Maeo S, Krämer M, Utaka T and Taniguchi K 2009 *X-ray Spectrometry* **38** 333

[14] Verhoff B, Harilal S S, Freeman J R, Diwakar P K and Hassanein A 2012 *J. Appl. Phys.* **112** 093303

[15] Osterholz J, Brandl1 F, Cerchez M, Fischer T, Hemmers D, Hidding B, Pipahl A, Pretzler G, Rose S J and Willi O 2008 *Phys. Plasmas.* **15** 103301

[16] Ma Q, Motto-Ros V, Laye F, Yu J, Lei W, Bai X, Zheng L and Zeng H 2012 *J. Appl. Phys.* **111** 053301

[17] Bartnik A, Wachulak P, Fok T, Wegrzyński Ł, Fiedorowicz H, Pisarczyk T, Chodukowski T, Kalinowska Z, Dudzak R, Dostal J, Krousky E, Skala J, Ullschmied J, Hrebicek J and Medrik T 2015 *Phys. Plasmas.* **22** 043302

[18] Wu T, Higashiguchi T, Li B, Suzuki Y, Arai G, Dinh T H, Dunne P, O'Reilly F, Sokell E and O'Sullivan G 2015 *J. Phys. B* **48** 245007

[19] Harte C S, Higashiguchi T, Otsuka T, D'Arcy R, Kilbane D and O'Sullivan G 2012 *J. Phys. B* **45** 205002

[20] Yuan R, Tang Y, Zhu Z H, Hao Z Q, Li J M, Yu H Y, Yu Y X, Guo L B, Zeng X Y and Lu Y F 2019 *Anal. Chim. Acta* **1064** 11

[21] Cann N M and Thakkar A J 1992 *Phys. Rev. A* **46** 5397

[22] Costello J T, Kennedy E T, Mosnier J-P, Sayyad M H and Mcguinness C 1998 *J. Phys. B: At. Mol. Opt. Phys.* **31** L547

[23] Gao X, Song X W, Tao H Y, Lin J Q and Guo K M 2011 *Acta Phys. Sin.* **60** 025203 (in Chinese)

[24] Su M G, Cao S Q, Sun D X, Min Q and Dong C Z 2016 *Phys. Plasmas.* **23** 033302

[25] Su M G, Cao S Q, Sun D X, Min Q and Dong C Z 2016 *Chin. Phys. Lett.* **33** 45201

[26] Li F, Liang G Y and Zhao G 2013 *Astrophys. J.* **762** 53

[27] Tully J A, Seaton M J and Berrington K A 1990 *J. Phys. B* **23** 3811

[28] Cao S Q, Su M G, Min Q, Sun D X, O'Sullivan G and Dong C Z 2018 *Phys. Plasmas.* **25** 023304

[29] http://www.nist.gov (the NIST Atomic Spectra Database Lines Form) [2019-3-13]

[30] Cowan R D 1981 *The Theory of Atomic Structure and Spectra* (Berkeley: University of California Press)

[31] Gu M F 2008 *Can. J. Phys.* **86** 675

[32] Colombant D and Tonon G F 1973 *J. Appl. Phys.* **44** 3524